minerals

MDPI

Article

In Situ U-Pb Geochronology of Calcite from the World's Largest Antimony Deposit at Xikuangshan, Southern China

Junwei Xu [1,2], Xianghua Liu [2,*], Jianqing Lai [2], Hongsheng He [1], Xiangfa Song [2], Degao Zhai [3], Bin Li [2], Yuhua Wang [2], Jian Shi [4] and Xi Zhou [4]

[1] The Coal Geological Exploration Institute of Hunan Province, Changsha 410000, China; 12021191@csu.edu.cn (J.X.); amazeboa@163.com (H.H.)
[2] Key Laboratory of Metallogenic Prediction of Nonferrous Metals and Geological Environment Monitoring, Ministry of Education, School of Geosciences and Info-Physics, Central South University, Changsha 410083, China; ljq@csu.edu.cn (J.L.); xfsong@csu.edu.cn (X.S.); cutelb@csu.edu.cn (B.L.); 18349271135@163.com (Y.W.)
[3] State Key Laboratory of Geological Processes and Mineral Resources, China University of Geosciences, Beijing 100083, China; dgzhai@cugb.edu.cn
[4] Geological Bureau of Hunan Province, Changsha 410083, China; tanshijian@163.com (J.S.); zhouxixicsu@163.com (X.Z.)
* Correspondence: xianghua@csu.edu.cn; Tel.: +86-132-1133-6907

Abstract: The Xikuangshan antimony (Sb) deposit is the world's largest known Sb deposit. Due to the lack of suitable minerals for reliable high-precision radiometric dating, it remains difficult to determine the exact age of Sb mineralization in this deposit. Here, we report the first LA-MC-ICP-MS U-Pb ages of syn-stibnite calcite from this deposit. The dating results indicate the presence of at least two stages of Sb mineralization in the Xikuangshan ore district. The calcite-stibnite veins in the Daocaowan ore block probably formed during the Paleocene (58.1 ± 0.9 Ma), representing an early stage of Sb mineralization, while the quartz-stibnite vein in the Feishuiyan ore block probably formed during the Eocene (50.4 ± 4.4 Ma, 50.4 ± 5.0 Ma, and 51.9 ± 1.6 Ma), representing a late stage of Sb mineralization. The new calcite U-Pb ages are significantly younger than the calcite Sm-Nd ages (124.1 ± 3.7 Ma, 155.5 ± 1.1 Ma) reported by previous researchers. We suggest that Sb mineralization of the South China antimony metallogenic belt may be related to tectono-thermal events during Paleogene, possibly linked to high heat flow during the subduction (ca. 60–40 Ma) of the Pacific Plate beneath the Eurasian Plate and/or the Indo–Asian Collision (began at ca. 61 Ma). The young in situ U-Pb ages of calcite challenge the idea of late Mesozoic Sb mineralization in the South China antimony metallogenic belt, suggesting the requirement for more high-precision dating studies.

Keywords: Xikuangshan antimony deposit; calcite; U-Pb geochronology; antimony mineralization; south China

Citation: Xu, J.; Liu, X.; Lai, J.; He, H.; Song, X.; Zhai, D.; Li, B.; Wang, Y.; Shi, J.; Zhou, X. In Situ U-Pb Geochronology of Calcite from the World's Largest Antimony Deposit at Xikuangshan, Southern China. *Minerals* **2022**, *12*, 899. https://doi.org/10.3390/min12070899

Academic Editor: Simon Paul Johnson

Received: 16 June 2022
Accepted: 14 July 2022
Published: 18 July 2022

1. Introduction

Antimony (Sb) is an important mineral commodity widely used in industry and military applications, and is listed as a critical metal by the United States, China, and other countries [1–3]. Sb resources are unequally distributed around the world. China has the bulk of the world's identified Sb resources, which are concentrated in the South China antimony metallogenic belt. The Xikuangshan Sb deposit is the largest Sb deposit that has been discovered in this belt and also the largest currently known in the world. The high-precision mineralization age of such a giant Sb deposit plays an important role in understanding its genesis and helping to further regional prospecting, for example, whether it is linked to the coeval granitic magmatism or tectonic events.

Most researchers currently believe that Sb mineralization in the Xikuangshan ore district occurred in the late Mesozoic, and two stages of Sb mineralization (124.1 ± 3.7 Ma and 155.5 ± 1.1 Ma, respectively) were derived from the calcite Sm-Nd dating method by Peng et al. [4,5]. However, recently, Tang et al. [6] applied a high-precision in situ scheelite LA-ICP-MS U-Pb dating method at the Woxi Sb-Au-W deposit and obtained new mineralization ages (ca. 142.7–144.3 Ma), which are significantly different from the previously reported scheelite Sm-Nd age (402 ± 6 Ma [7]). Additionally, in situ U-Pb ages of wolframite (145.6 ± 2.1 Ma) and apatite (144.8 ± 1.5 Ma) obtained by Li et al. [8] also show much younger ages than the scheelite Sm-Nd age at the Woxi Sb-Au-W deposit. This indicates that Sm-Nd dating results obtained by previous application of HF and $HClO_4$ dissolution of whole minerals (calcite or scheelite) appear to yield overly old ages of mineralization. Another noteworthy disadvantage of the traditional calcite Sm-Nd dating method [4,5] is that multiple generations of mineralization cannot be distinguished in situ within an individual calcite crystal or vein. Additionally, Jin et al. [9] performed electron spin resonance (ESR) age determination on syn-stibnite quartz samples from quartz-stibnite veins and revealed that Sb mineralization ranged from 66.4 to 51.6 Ma. Moreover, Luo et al. [10] proposed an LA-MC-ICP-MS calcite U-Pb age of 60.0 ± 0.9 Ma in the Weizhai Sb deposit, suggesting that a potential tectonothermal event occurred in the South China antimony metallogenic belt during Paleogene. It is noteworthy that a small amount of Sb mineralization was also found in the red sandstone of the upper Daijiaping Formation of the Upper Cretaceous [9]. All these indicate that the age of Sb mineralization may be later than the Yanshanian period (late Jurassic and early Cretaceous). In order to better constrain the age of Sb mineralization in the Xikuangshan ore district, our team decided to carry out high-precision dating and finally adopted the calcite LA-MC-ICP-MS in situ U-Pb dating method for the following reasons: (1) The Xikuangshan Sb deposit has a large amount of syn-stibnite calcite with developed crystals and low inclusions. (2) In recent years, the calcite LA-MC-ICP-MS in situ U-Pb dating method has been greatly developed to achieve low Pb detection limits (ca. 1 ppb Pb) and high spatial resolution (ca. 100 μm) [11–17], and successfully applied to geochronological studies in an increasing number of cases [10,18–20], showing great potential.

The goal of this research was to apply a high-precision dating method to solve the challenging problem of Sb mineralization age in the Xikuangshan Sb deposit, as well as to investigate Sb mineralization generations and genesis of the South China antimony metallogenic belt.

2. Geological Background

2.1. Regional Geology

The Xikuangshan Sb deposit is located in central Hunan province, South China. Tectonically, it is situated in the South China Block, which comprises the Cathaysia Block to the southeast and the Yangtze Block to the northwest, and was amalgamated together along the Jiangshao suture zone at ~880 Ma (Figure 1a; [21]).

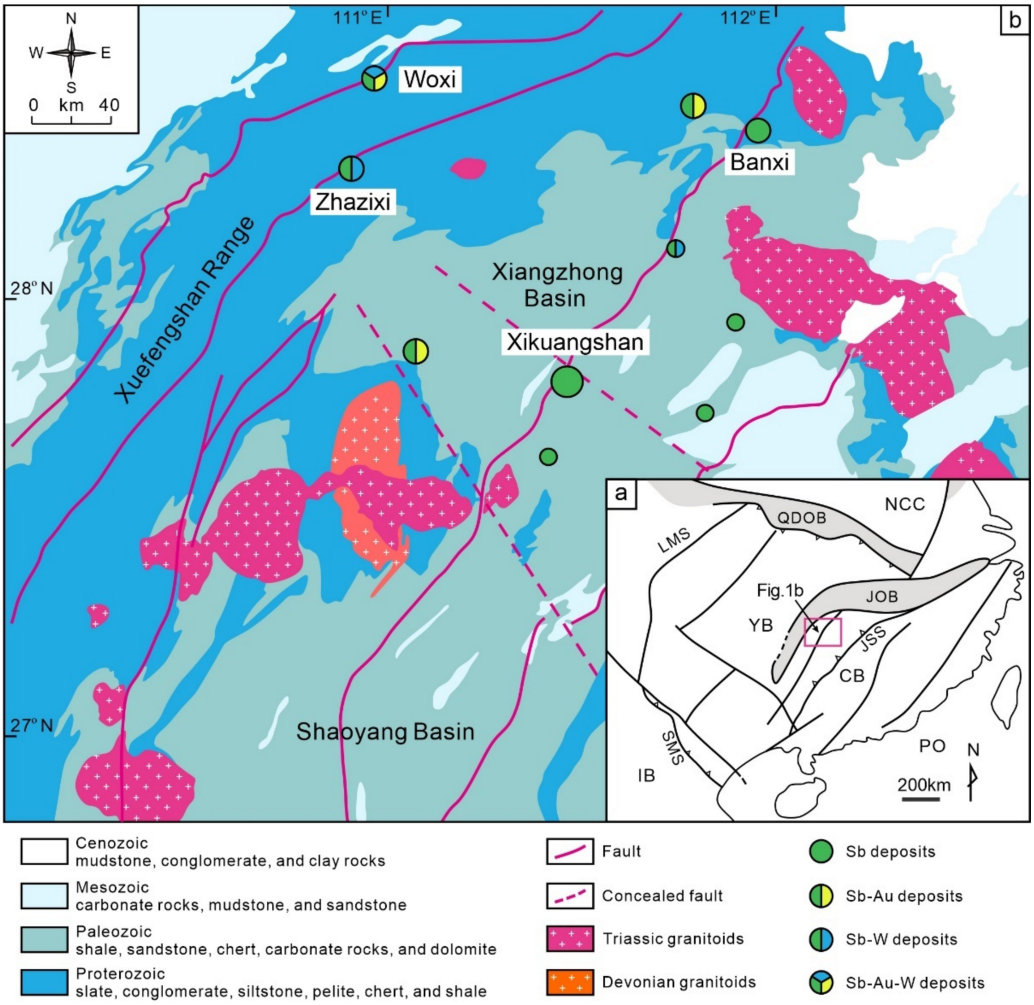

Figure 1. (**a**) Tectonic map showing the location of the Xiangzhong metallogenic province in southern China (modified after [21,22]). Symbols: NCC = North China Craton, QDOB = Qinling–Dabie Orogen Belt, LMS = Longmenshan Fault, JOB = Jiangnan Orogen Belt, YB = Yangtze Block, JSS = JiangShao Suture, CB = Cathaysia Block, SMS = Song-MA Suture, IB = Indochina Block, PO = Pacific Ocean. The thick black lines represent the main boundary faults. The serrated shape represents the suture zone. The thin black lines represent the coastline. (**b**) Regional geologic map of the Xikuangshan Sb deposit, showing the distribution of important Sb deposits in Xiangzhong metallogenic province (modified after [21,22]).

The Xiangzhong metallogenic province mainly includes the Xikuangshan Sb deposit, Zhazixi Sb-W deposit, Woxi Sb-Au-W deposit, and Banxi Sb deposit, which is the northwest section of the South China antimony metallogenic belt [10,23]. To present, abundant Sb-(Au-W) deposits have been discovered in this region, with more than 170 Sb-(Au-W) ore deposits and prospects [21,22]. The Xiangzhong metallogenic province is mainly comprised of the Xuefengshan Range and the Xiangzhong Basin, and is located southwest of the Jiangnan Orogen Belt (Figure 1b). The basement of this region is mainly composed of Neoproterozoic (slate, conglomerate, siltstone, pelite, chert, and shale) and Paleozoic (shale, sandstone, chert, carbonate rocks, and dolomite) low-grade metasedimentary rocks, whereas the overlying sedimentary rocks mainly consist of Mesozoic-to-Cenozoic clastic and carbonate rocks (Figure 1b). Igneous rocks in this region are dominated by Triassic granitoids (ca. 250–200 Ma) and Devonian granitoids (ca. 420–360 Ma), which are mostly observed in outcrop at the margins of the Xiangzhong basin and Shaoyang basin (Figure 1b) [21]. There is a lack of igneous rocks within the Sb ore districts, with only a small proportion of lamprophyre and felsic porphyries dikes in some Sb deposits. There is no evidence

for an apparent genetic connection between magmatic rocks and regional Sb mineralization [4,24,25]. The fault structures are mainly NE- and NW-trending. The Xikuangshan Sb deposit is situated at the intersection of the NE-trending Taojiang–Chengbu regional fault and the NW-trending Xikuangshan–Lianyuan concealed fault (Figure 1b) [26].

2.2. Ore Deposit Geology

The sedimentary strata of the Xikuangshan ore district consists mainly of the Upper Devonian and Lower Carboniferous (Figure 2a).

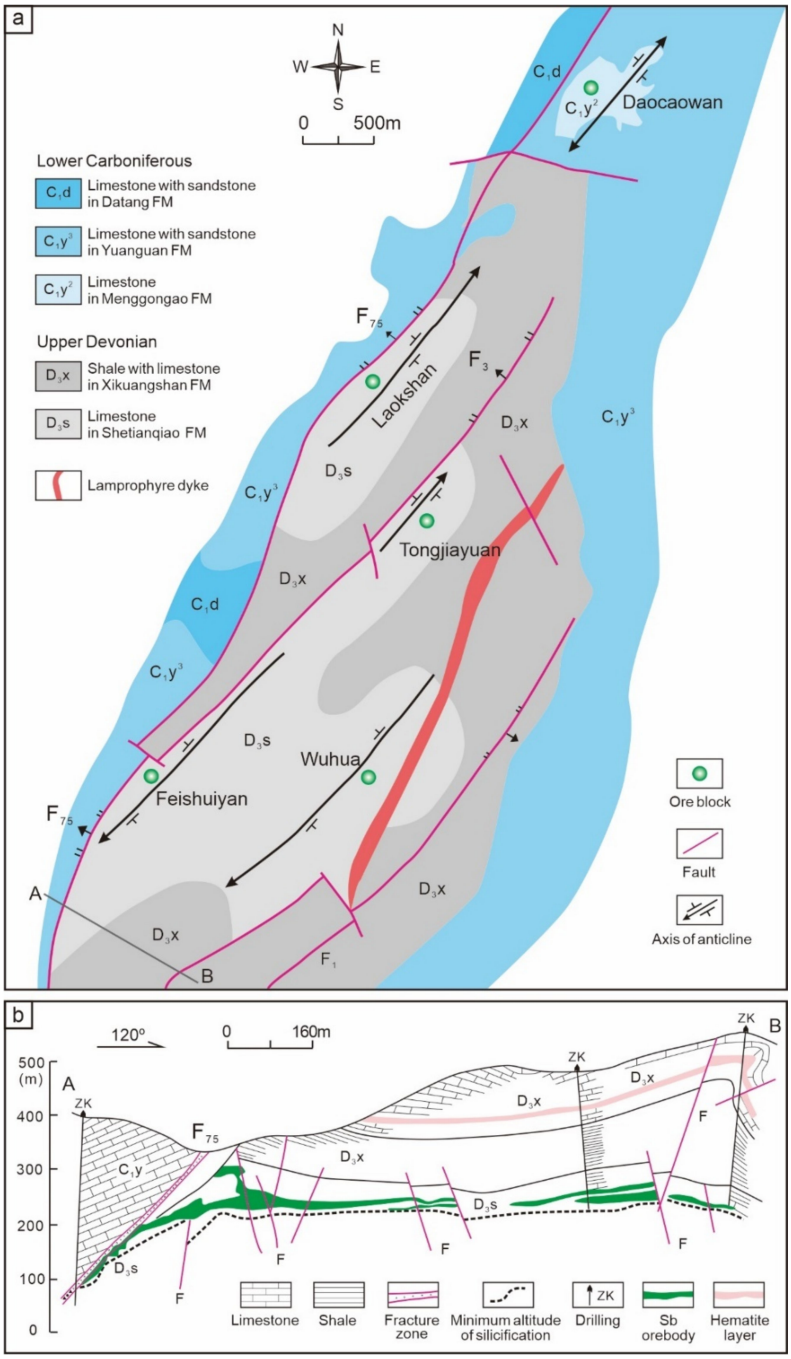

Figure 2. (**a**) Simplified geologic map of the Xikuangshan Sb deposit (modified after [27]). There are five ore blocks in the Xikuangshan Sb deposit: Daocaowan, Laokuangshan, Tongjiayuan, Wuhua, and Feishuiyan. (**b**) A representative section of the Xikuangshan Sb deposit showing the geological and geometric characteristics of Sb orebodies (modified after [27,28]).

The Upper Devonian includes the Shetianqiao (D_3s) and Xikuangshan (D_3x) Formation. The Shetianqiao Formation, conformably underlying the Xikuangshan Formation, comprises predominately of limestone, locally accompanied by shale. The Xikuangshan Formation is composed of interbedded shale and carbonate with a hematite layer (Figure 2b). The younger strata in the Xikuangshan ore district include the Lower Carboniferous Menggongao (C_1y^2), Yanguan (C_1y^3), and Datang (C_1d) Formation, which were locally interbedded with limestone and sandstone (Figure 2a).

There are almost no igneous rocks in the Xikuangshan ore district. Only one NNE-trending lamprophyre dike was observed in the eastern part of the district (Figure 2a) [5]. This lamprophyre dike has a biotite K-Ar age of 128 Ma [29]. Researchers generally accept that there is no genetic relationship between magmatism and Sb mineralization in the Xikuangshan Sb deposit [21,26,30].

The Sb mineralization in the Xikuangshan district is mainly constrained by five en échelon second-order anticlines of the Xikuangshan complex anticline, including five ore blocks of Daocaowan, Laokuangshan, Tongjiayuan, Wuhua, and Feishuiyan. The northwest limb of the Xikuangshan complex anticline is cut by the NE-trending fault F_{75}, which is a part of the Taojiang–Chengbu regional deep fault. Almost all the Sb orebodies occur in the footwall of fault F_{75}, which is assumed to be the main channel for migration of Sb mineralizing fluids (Figure 2) [31].

The Xikuangshan Sb deposit is dominated by five ore blocks, i.e., Daocaowan, Laokuangshan, Tongjiayuan, Wuhua, and Feishuiyan (Figure 2a) [5]. The Sb mineralization in the Daocaowan ore block is an important discovery in recent years [32]. Most Sb orebodies occur typically in stratiform under the organic-rich shale in the lowermost part of the Xikuangshan Formation and are mainly in the silicified fossil-rich limestone of the Shetianqiao Formation, all above the minimum altitude of silicification (Figure 2b). Notably, all Sb mineralization strictly within the silicified zone of limestone. In addition, all silicification occur along the footwall of the fault F_{75} (or secondary faults parallel to F_{75}), and the intensity of silicification increases significantly toward the fault [28]. The shape of individual stibnite veins is usually network-like, irregular, or veinlet-like, and rarely shows concordance with the host Upper Devonian strata (Figure 3a,b).

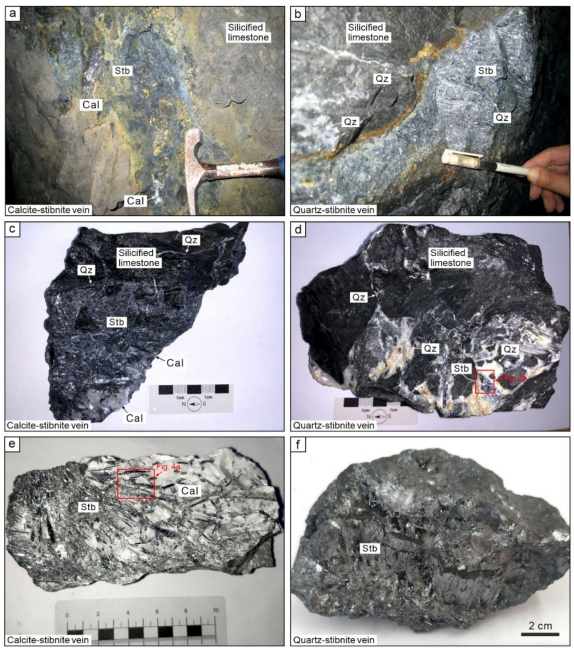

Figure 3. Representative photographs of orebodies and Sb ores in the Xikuangshan Sb deposit. The host rock of both quartz-stibnite vein and calcite-stibnite is silicified limestone. (**a**,**c**,**e**) Calcite-stibnite vein and hand specimens. (**b**,**d**,**f**) Quartz-stibnite vein and hand specimens. Abbreviations: Qz = quartz, Cal = calcite, Stb = stibnite.

The irregular orebodies are mainly distributed at the depth of the Shetianqiao Formation (Figure 2b). The Sb orebodies extend 30–600 m along strike and dip downward 1300–1800 m, with a thickness of 1–5 m, locally up to 20 m thick. Ore grades for Sb generally range from 3.5 to 5.7 wt% Sb, averaging 4.0 wt% [28,33].

Sb ores in the Xikuangshan ore district are massive, network-like, brecciated, and disseminated [28]. The mineralogy of the ores is simple: stibnite is the only ore mineral, and quartz and calcite are the main gangue minerals (Figures 3 and 4), in addition to minor amounts of fluorite, barite, and talc [28].

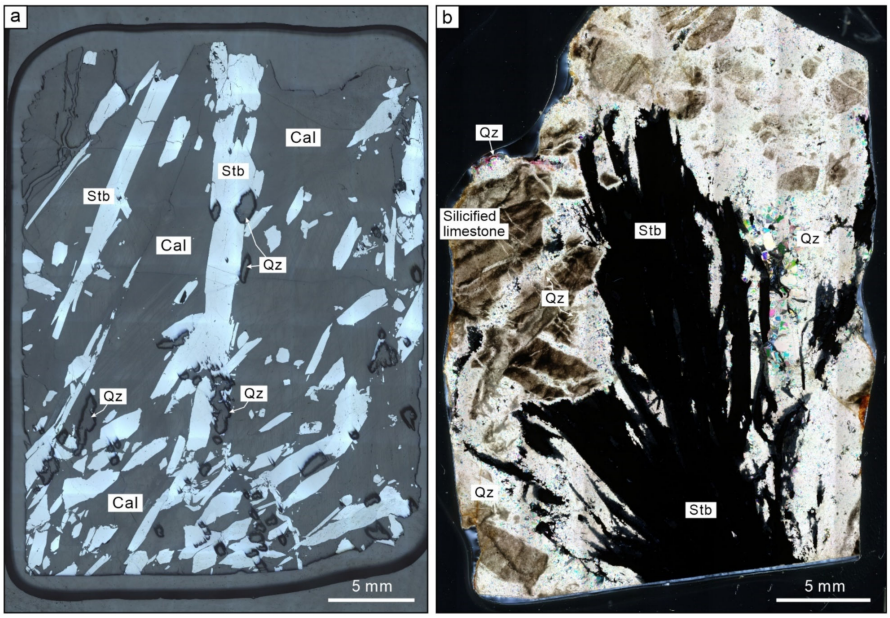

Figure 4. Representative thin section images of Sb ores. (**a**) Photomicrograph of calcite-stibnite vein under reflected light. (**b**) Photomicrograph of quartz-stibnite vein under plane-polarized light. Abbreviations as in Figure 3.

Previous studies suggest that the ore types in the Xikuangshan Sb deposit can be divided into early-stage and late-stage Sb mineralization [24,34,35]. The early-stage Sb mineralization formed quartz-stibnite veins, fluorite-quartz-stibnite veins, and barite-quartz-stibnite veins, and the late-stage Sb mineralization formed calcite-stibnite veins [28]. The quartz-stibnite veins of early-stage Sb mineralization are the most important ore type, accounting for more than 80% of Sb ore reserves throughout the Xikuangshan ore district. The Sm-Nd isotopic ages of syn-stibnite calcite are 155.5 ± 1.1 Ma and 124.1 ± 3.7 Ma, representing early-stage and late-stage Sb mineralization ages, respectively [4,5]. Additionally, two (U-Th)/He age populations, 156–117 and 97–86 Ma, were obtained from detrital zircons from the altered host rocks (silicified limestone) of quartz-stibnite veins in the Xikuangshan Sb deposit [22]. Fu et al. (2020) argued that the older age population (156–117 Ma) probably represents the timing of main-stage Sb mineralization, while the younger ages (97–86 Ma) may result from partial loss of He in zircon caused by the distal effect of deep-seated intrusions beneath the deposit. In order to better constrain the age of Sb mineralization in the Xikuangshan Sb deposit, we collected samples from the quartz-stibnite veins and calcite-stibnite veins (Figure 3), representing two stages Sb mineralization. The mineral assemblage of the calcite-stibnite veins is predominantly calcite and stibnite, but with a few fine-grained quartz crystals on the edges of the euhedral-subhedral stibnite crystals (Figures 4a and 5a).

The quartz-stibnite veins comprise mainly of quartz and stibnite (Figure 4b), with calcite locally present (Figure 6a,b,e).

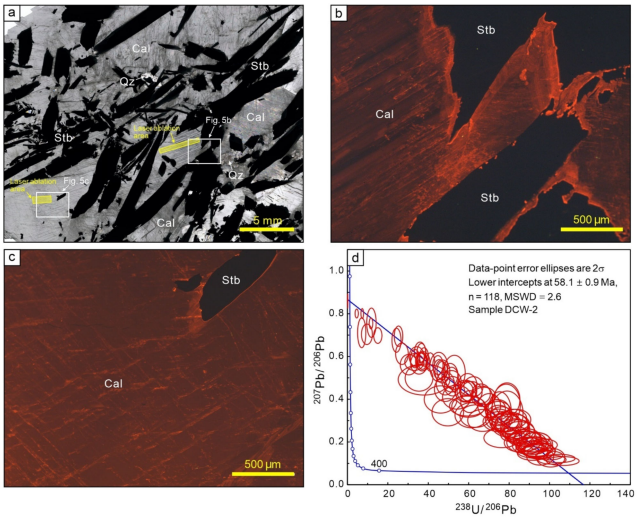

Figure 5. (**a**) Photomicrograph showing the calcite coexisting with stibnite (sample DCW-2, under plane-polarized light) in calcite-stibnite vein, and the areas of LA-MC-ICP-MS calcite U-Pb isotope analyses (yellow area). (**b**,**c**) Cathodoluminescence (CL) images of syn-stibnite calcite crystals from the Xikuangshan Sb deposit. (**d**) Tera–Wasserburg concordia diagram of LA-MC-ICP-MS U-Pb data of syn-stibnite calcite crystals in calcite-stibnite vein. Error ellipses are at 2σ. MSWD = mean standard weighted deviation. Abbreviations as in Figure 3.

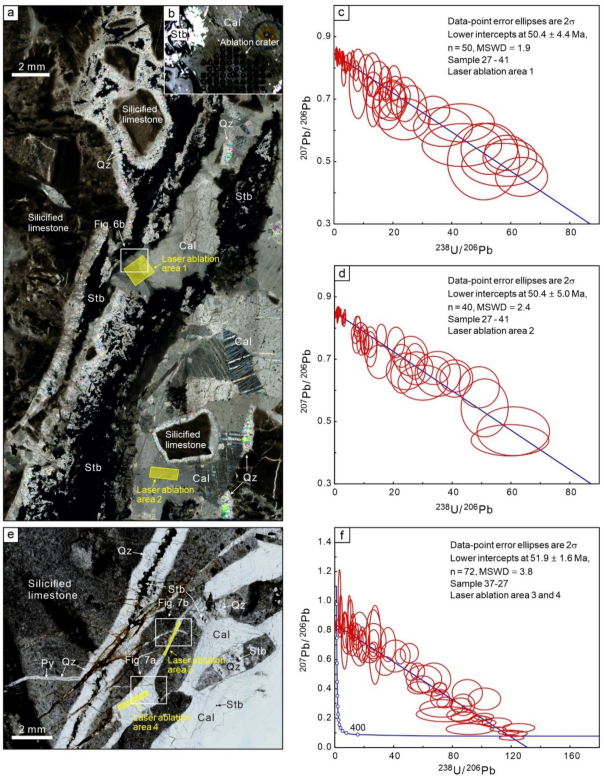

Figure 6. (**a**) Photomicrograph showing the occurrence of stibnite, calcite, and quartz in quartz-stibnite vein (sample 27–41, under plane-polarized light) from the Xikuangshan Sb deposit, and the areas of LA-MC-ICP-MS calcite U-Pb isotope analyses (yellow area). (**b**) Representative laser ablation craters. (**c**,**d**) Tera–Wasserburg concordia diagrams of syn-stibnite calcite crystals in the laser ablation areas 1 and 2, respectively. (**e**) The mineral assemblage in quartz-stibnite vein (sample 37–27, under plane-polarized lights), and the areas analyzed for U-Pb dating (yellow area). (**f**) Tera–Wasserburg concordia diagram of syn-stibnite calcite crystals in the laser ablation areas 3 and 4. Error ellipses are at 2σ. Py = pyrite, other abbreviations as in Figure 3.

3. Sample Preparation and Calcite Occurrence

3.1. Samples

All samples were collected from underground exposures in this study. Fresh stibnite-bearing samples have been collected for calcite U-Pb dating from the Daocaowan and Feishuiyan ore blocks, representing the north and south ore blocks of the Xikuangshan Sb deposit, respectively. One sample was collected in calcite-stibnite vein from the Daocaowan ore block, numbered DCW-2. Two samples were collected in quartz-stibnite vein from the Feishuiyan ore block, numbered 27–41 and 37–27, respectively. The samples collected in this study represented two types of Sb ores: calcite-stibnite veins and quartz-stibnite veins. Field photographs of samples are shown in Figure 3a,b.

3.2. Calcite Occurrence

In the calcite-stibnite veins, calcite occurs as massive, breccia, and vein with coarse-grained euhedral stibnite crystals (Figure 3a,c,e). Calcite in the calcite-stibnite veins is commonly penetrated by euhedral stibnite crystals. which suggests cogenetic precipitation of calcite and stibnite (Figure 4a). In the quartz-stibnite veins, calcite crystals account for significantly less volume fraction than in the calcite-stibnite veins (Figure 3b,d,f) and is present as gangue mineral in Sb mineralization. In the quartz-stibnite veins, calcite is intergrown with fine-grained stibnite and fine-grained quartz (Figure 6a). Locally, calcite is penetrated by euhedral stibnite crystal, encasing silicified limestone breccia (Figure 6a,b), containing inclusions of stibnite (Figure 6e), all of which show characteristics of syn-stibnite calcite.

Using cathodoluminescence (CL) imaging, calcite in the calcite-stibnite veins is relatively homogeneous, with high CL intensity, and displays a bright orange luminescence (Figure 5b,c). Calcite in the quartz-stibnite veins is relatively inhomogeneous, with low CL intensity, and displays a mottled orange luminescence (Figure 7).

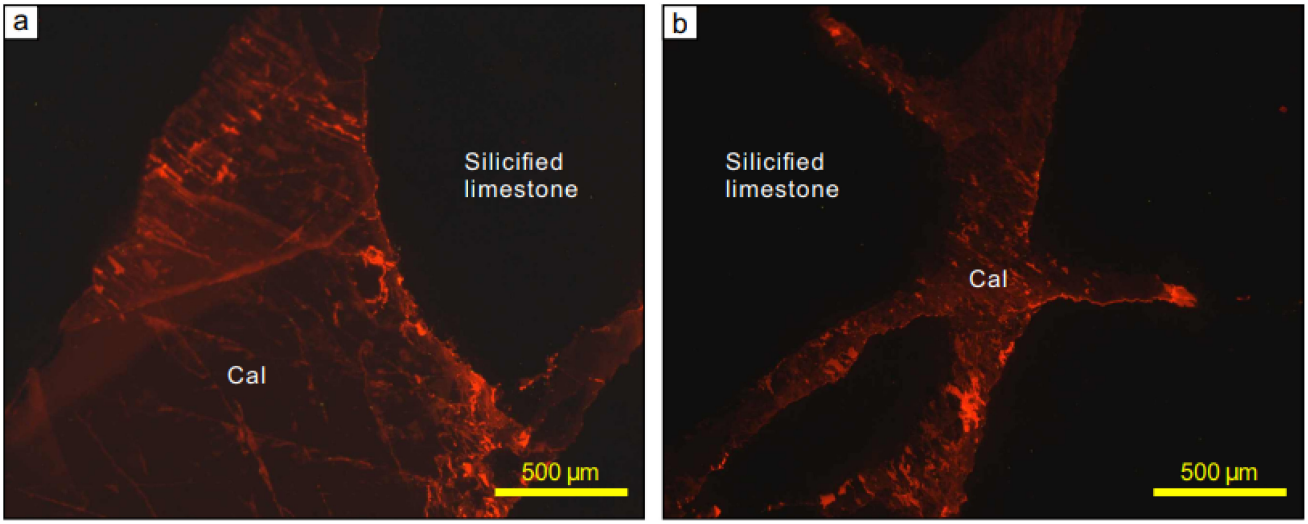

Figure 7. CL images of syn-stibnite calcite crystals in quartz-stibnite vein from the Xikuangshan Sb deposit (sample 37–27). (**a**) CL image of part of laser ablation area 4. (**b**) CL image of part of laser ablation area 3. The location is shown in Figure 6e. Abbreviations as in Figure 3.

It is remarkable that both types of calcites show higher CL intensity at the joints and crystal boundaries.

4. Analytical Methods

4.1. Cathodoluminescence (CL) Imaging

Prior to the analyses, the investigation of calcite internal textures by CL imaging was performed at the Key Laboratory of Metallogenic Prediction of Nonferrous Metals and Geological Environment Monitoring (Ministry of Education), Central South University, Changsha, China. It was performed under a Zeiss A1 microscope coupled with CFL-2 Cathode luminescence. The high voltage ranges used in this experiment ranged from 6 kV to 15 kV, and the current ranges were from 220 μA to 380 μA.

4.2. LA-MC-ICP-MS Calcite U-Pb Isotope Analyses

In situ U-Pb isotopic analysis was conducted at Micro-Origin and Spectrum Laboratory (Sichuan Chuanyuan Weipu Analytical Technology Co. Ltd., Chengdu, China) using a Thermo Scientific quadrupole iCap TQ inductively coupled plasma mass spectrometer (Q-ICP-MS) coupled with an ASI Resolution LR 193 nm ArF excimer laser ablation (LA) system. The unknowns were calculated by interpolating the measurement/acceptance ratios of NIST-614 glass, as well as the instrumental drift and partial bias in the $^{238}U/^{206}Pb$ ratio (Figure S1a) [36]. Glass NIST 614 was used as a primary reference material, which bracketed carbonate reference materials and the unknowns at every five intervals to correct for the $^{207}Pb/^{206}Pb$ ratios of the reference. The $^{238}U/^{206}Pb$ ratios of calcite samples were then further calibrated with an in-house standard (AHX-1d, 238.2 ± 0.9 Ma; Figures S2 and S5). In addition, to ensure age reliability and accuracy, cross-checks were performed with an ID-MS calibrated calcite standard PTKD-2 (153.7 ± 1.7 Ma; Figures S3 and S6) [20] and an in-house intensive LA calibrated standard (LD-5, 72.5 ± 1.0 Ma; in press; Figures S4 and S7). In this experiment, the PTKD-2 and LD-5 calcite standards anchored using a $^{207}Pb/^{206}Pb$ value of value of 0.85 [20]. A spot ablation mode with an ablation speed of 3.0 J/cm^2, a frequency of 15 Hz, and a spot size of 120 μm were applied in this study (Figure S1b,c). The laser timing was set with 2 s surface cleaning, 7 s washout, 15 s background, 20 s of ablation, and 6 s washout. The experimental setup and methods are described elsewhere in detail [10,14,16].

5. Results

In situ U-Pb dating for syn-stibnite calcite in the calcite-stibnite vein from the Daocaowan ore block (sample DCW-2) obtained datable U/Pb ratios (0.04–63) with 31–390 ppb U (mean 216 ppb) and 3–930 ppb Pb (mean 78 ppb; Table S1; Figure 8).

As shown in Figure 5d, calcite in the calcite-stibnite vein has 118 spots with U-Pb data falling on well-defined lines in the Tera–Wasserburg concordia diagram (data-point error ellipses are 2σ) and yields an age of 58.1 ± 0.9 Ma (MSWD = 2.6).

Syn-stibnite calcite in the quartz-stibnite vein from the Feishuiyan ore block (samples 27–41 and 37–27) have datable U/Pb ratios (0.10–66.9) with 11–733 ppb U (mean 236 ppb) and 3–2095 ppb Pb (mean 152 ppb; Table S1). The U/Pb ratios of calcite from the two different veins vary in a similar range, but the U content of calcite in quartz-stibnite veins is relatively more variable (Figure 8). Syn-stibnite calcite in laser ablation area 1 of sample 27–41 has an isochron defined by 50 U-Pb data points, with a highly radiogenic lower intercept age of 50.4 ± 4.4 Ma (MSWD = 1.9; Figure 6a,c). An isochron defined by 40 U-Pb data points is found in laser ablation area 2 of sample 27–41, with a lower intercept age of 50.4 ± 5.0 Ma (MSWD = 2.4; Figure 6a,d). Syn-stibnite calcite in laser ablation areas 3 and 4 of sample 37–27 has an isochron defined by 72 U-Pb data points, with a lower intercept age of 51.9 ± 1.6 Ma (MSWD = 3.8; Figure 6e,f).

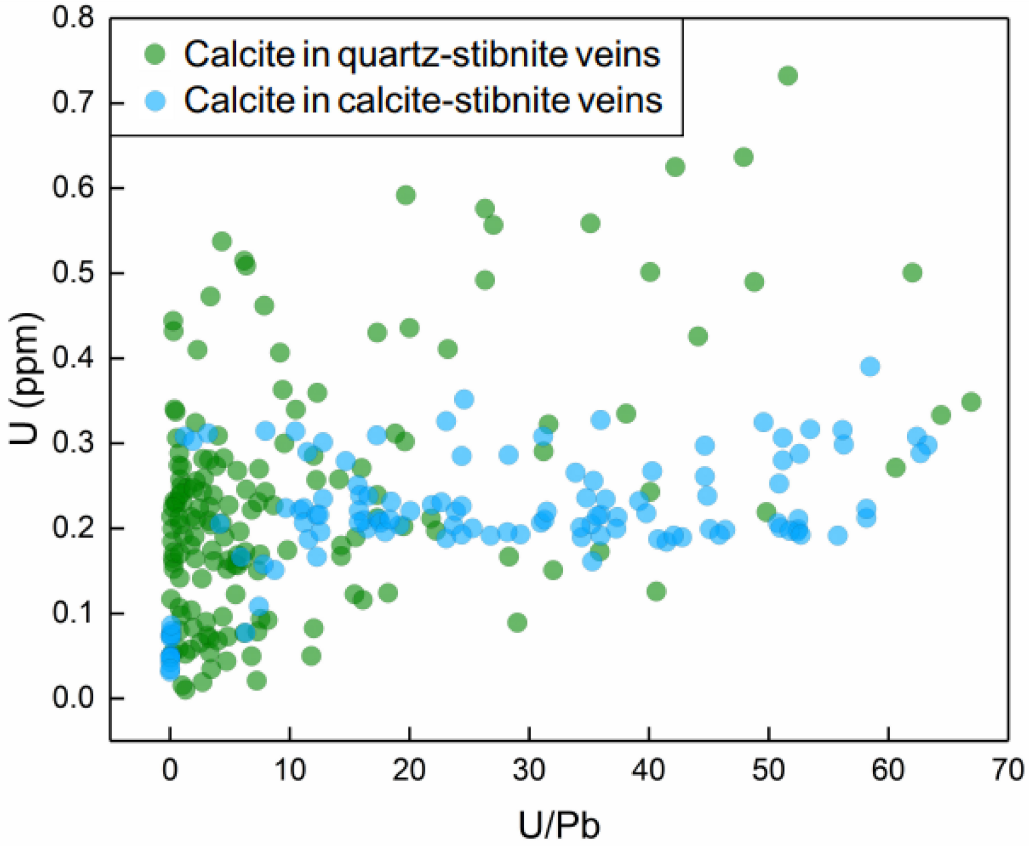

Figure 8. Plots of U content versus U/Pb ratios for two stages of calcite from the Xikuangshan Sb deposit.

6. Discussion

6.1. Reliability of Calcite U-Pb Age

As mentioned above, the U and Pb contents of calcite from the Xikuangshan Sb deposit are less than 1 ppm, which makes it difficult to measure the age reliably using traditional Q-ICP-MS or MC-ICP-MS [37]. During the experiment, we employed an electron multiplier discrete dynode multiplier dedicated to static measurement of low signal ^{238}U at the highest mass end of the collector array of the Nu Plasma II MC-ICP-MS. This discrete dynode multiplier has a higher sensitivity (100 μm, 3 J/cm^2, 10 Hz; ^{238}U > 500,000 cps/ppm, ^{207}Pb blank = 10–100 cps), which is about 3–10 times higher than that of Q-ICP-MS [10,38–40].

Our employment of LA-MC-ICP-MS obtained good signal intensities for the low-U and -Pb calcite samples and achieved acceptable internal errors for U and Pb isotopic compositions in this study. As shown in the Tera–Wasserburg concordia diagrams ($^{238}U/^{206}Pb$-$^{207}Pb/^{206}Pb$; Figures 5d and 6c,d,f), the scatters (MSWD = 2.6, 1.9, 2.4, and 3.8) of U and Pb isotopic compositions are over-dispersed and yield MSWD >1 following uncertainty propagation. Possible explanations for this include: (1) mobilization of U and/or Pb within or among calcite crystals after crystallization (e.g., Pb- or U-loss); (2) partial resetting of the U-Pb systematics through recrystallization and/or diffusion of U and/or Pb in calcite crystals; (3) fluid inclusions and/or impurities were mixed and sampled during ablation; (4) mixed sampling of calcite crystals of different generations during ablation; and (5) very low U and Pb content of calcite with relatively large uncertainties on individual measurements (low U and Pb signals). The first to third scenarios cannot be entirely ruled out. However, few analyses in the samples very clearly deviate from the near-colinear arrays, yielding slightly younger or older age components (Figures 5d and 6c,d,f). The fourth scenario can be ruled out, since the ablated calcite crystals are homogeneous in both photomicrographs and CL images (Figures 4–7). The most likely explanation is the fifth scenario, since the MSWD values of the secondary standards in the different calcite U-Pb dating experiments [18] are

beyond the range suggested for the U-rich accessory minerals such as zircon and monazite, and do not correlate with the number of analyses (*n*) for each sample. Therefore, the slightly higher MSWD values (1.5–3.8) for the calcite U-Pb dating results of the Xikuangshan Sb deposit are likely due to the very low U and Pb content (<10 ppb) in calcite. Besides, through cross-calibration by AHX-1d (Figures S2 and S5; Table S2), the matrix-matched carbonate reference materials PTKD-2 (153.7 ± 1.7 Ma) [20] and LD-5 (72.5 ± 1.0 Ma) attained the expected ages within uncertainty (PTKD-2: 152.1 ± 2.1 Ma, MSWD = 3.0, 152.7 ± 3.5 Ma, MSWD = 2.7; LD-5: 72.8 ± 0.5 Ma, MSWD = 1.5, 72.5 ± 0.8 Ma, MSWD = 1.5; the data are shown in Figures S2–S7 and Table S2), confirming that the derived ages are reliable. Hence, the in situ calcite U-Pb ages obtained in the Xikuangshan Sb deposit are available.

6.2. Timing of Sb Mineralization in the Xikuangshan Sb Deposit

Calcite samples in both calcite-stibnite veins and quartz-stibnite veins from the Xikuangshan Sb deposit show characteristics of syn-stibnite calcite: penetrated by euhedral stibnite crystals, intergrown with stibnite, quartz, and silicified limestone, and locally containing silicified limestone breccia and stibnite. Additionally, Luo et al. [10] performed detailed LA-MC-ICP-MS calcite U-Pb dating for the Weizhai Sb deposit (located in the southwestern part of the South China antimony metallogenic belt) and argued that the U-Pb ages of syn-stibnite calcite can represent the timing of Sb mineralization, and suggested that this dating method is important for future use in age determination of hydrothermal ore deposits with extremely low U and Pb contents (<1 ppm) and a wide range of U/Pb ratio variations. Therefore, we suggest that the in situ U-Pb ages of syn-stibnite calcite from the Xikuangshan ore district may reveal the timing of Sb mineralization.

The calcite in situ LA-MC-ICP-MS U-Pb dating results indicate the presence of at least two stages of Sb mineralization in the Xikuangshan ore district. The calcite-stibnite veins in the Daocaowan ore block probably formed during the Paleocene (58.1 ± 0.9 Ma; Figure 5d), representing an early stage of Sb mineralization, while the quartz-stibnite veins in the Feishuiyan ore block probably formed during the Eocene (50.4 ± 4.4 Ma, 50.4 ± 5.0 Ma, 51.9 ± 1.6 Ma; Figure 6c,d,f), representing a late stage of Sb mineralization. The new U-Pb ages are significantly younger than the calcite Sm-Nd ages (124.1 ± 3.7 Ma, 155.5 ± 1.1 Ma) measured by Peng et al. [4,5] and zircon (U-Th)/He ages (97–86 Ma, 156–117 Ma) reported by Fu et al. [22] (Figure 9).

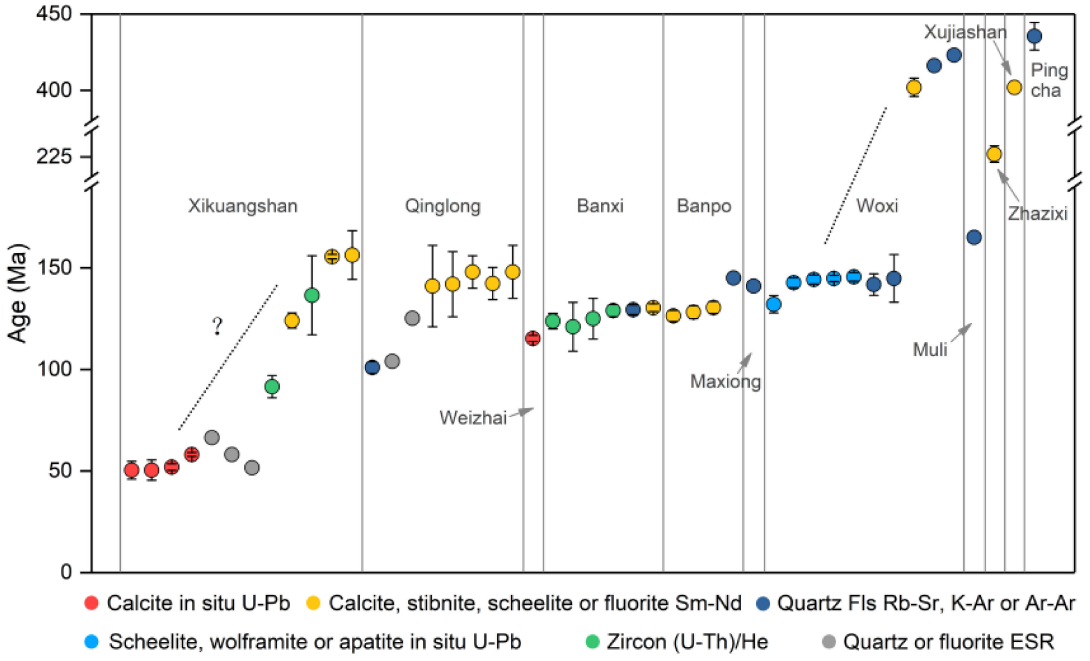

Figure 9. Age compilation of the South China antimony metallogenic belt (See Table 1 for details of data sources).

Table 1. Summary of Sb mineralization age of important Sb(-Au-W) deposits in the South China antimony metallogenic belt.

Ore Deposit	Host Strata	Host Rock	Ore-Type	Dating Method	Results (Ma)	References
Xikuangshan	Devonian	Carbonates, clastic rocks	Sb	Calcite in situ U-Pb	50.4 ± 4.4	This study
				Quartz ESR	50.4 ± 5.0 51.9 ± 1.6 58.1 ± 0.9 66.4 58.1 51.6	[9]
				Zircon (U-Th)/He	86–97	[22]
				Calcite Sm-Nd	117–156 124.1 ± 3.7 155.5 ± 1.1 156.3 ± 12	[5] [41]
Qinglong	Permian	Marine volcanic rocks	Sb-Au	Quartz Fls Rb-Sr	101.0 ± 2.9	[42]
				Fluorite ESR Quartz ESR	104 125.2	[43]
				Fluorite Sm-Nd	141 ± 20 142 ± 16 148 ± 8	[44] [5]
				Fluorite Sm-Nd Calcite Sm-Nd	142.3 ± 7.9 148 ± 13	[45]
Weizhai	Devonian-Silurian	Limestone, siltstone	Sb	Calcite in situ U-Pb	115.3 ± 1.5	[10]
Banxi	Neoproterozoic Banxi Group	Low-grade metamorphic rocks	Sb	Zircon (U-Th)/He	123.8 ± 3.8	[46]
Banpo	Devonian	Sandstones	Sb	Calcite Sm-Nd	121 ± 12 125 ± 10 129 ± 3	[47]
				Stibnite Rb-Sr	129.4 ± 2.4	[48]
				Stibnite Sm-Nd	130.4 ± 1.9	
				Calcite Sm-Nd	126.4 ± 2.7 128.2 ± 3.2 130.5 ± 3.0	[45] [42]
				Quartz Fls K-Ar	145	[49]
Maxiong	Cambrian, Devonian	Dolostones, sandstones	Sb	Quartz Fls Ar-Ar	141	[50]
Woxi	Neoproterozoic Banxi Group	Low-grade metamorphic rocks	Sb-Au-W	Scheelite in situ U-Pb	132.1 ± 4.3	[6]
				Apatite in situ U-Pb	142.7 ± 2.4 144.3 ± 2.2 144.8 ± 1.5	[8]
				Wolframite in situ U-Pb	145.6 ± 2.1	
				Quartz Fls Rb-Sr	141.8 ± 5.3 144.8 ± 11.7	[51]
				Scheelite Sm-Nd	402 ± 6	[7]
				Quartz Fls Ar-Ar	416.2 ± 0.8 423.2 ± 1.2	
Muli	Devonian	Carbonates	Sb	Quartz Fls Ar-Ar	165	[52]
Zhazixi	Neoproterozoic Banxi Group	Low-grade metamorphic rocks	Sb-W	Scheelite Sm-Nd	227.3 ± 6.2	[53]
Xujiashan	Upper Ediacaran	Carbonates, clastic rocks	Sb	Calcite Sm-Nd	402	[54]
Pingcha	Lower Ediacaran	Carbonates, clastic rocks	Sb	Quartz Fls Rb-Sr	435 ± 9	[55]

This would make the new ages reported in this study highly controversial, but it is necessary to point out that the previously measured ages of Sb mineralization in the Xikuangshan Sb deposit may be deficient as follows.

(1) The validity of Sm-Nd dating requires a fluid with homogeneous initial $^{143}Nd/^{144}Nd$ and minerals that have maintained closed systems with respect to Sm and Nd since crystallization [56]. Nevertheless, a study of the Yangjiashan vein-type W deposit by Li et al. [57] revealed that scheelite crystals have heterogeneous $^{143}Nd/^{144}Nd$ and $^{147}Sm/^{144}Nd$ composition (εNd values: −24.9 to −7.7). This is related to contamination of wall rocks with heterogeneous Nd isotope composition, challenges the significance of the absolute Sm-Nd ages, and requires micrometer- to nano-scale isotope analysis to obtain highly precise dating data [8,57]. Thus, this indicates that Sm-Nd isotope ages obtained by previous application of HF and $HClO_4$ dissolution of whole minerals (13 syn-stibnite calcites) [4,5] appear to yield insufficiently precise ages of Sb mineralization. (2) Two (U-Th)/He age populations of detrital zircon grains in the intensely silicified limestone from the Xikuangshan ore district were obtained by thermochronology [22]. Although the older zircon (U-Th)/He age population (156–117 Ma) are considered to possibly represent the timing of main-stage Sb mineralization in the Xikuangshan Sb deposit [22], it remains controversial whether the detrital zircon grains selected from the altered host rocks reflect the exact time of Sb mineralization [21]. Additionally, the geological significance of the younger zircon (U-Th)/He age population (97–86 Ma) remains unclear [22].

The LA-MC-ICP-MS calcite U-Pb ages obtained in this study from the Daocaowan ore block and the Feishuiyan ore block (ca. 58.1 Ma, 51.9–50.4 Ma, respectively) are very close to the quartz ESR ages measured by Jin et al. [9] at the Zuowan Sb deposit and the Laokuangshan ore block (58.1 Ma, 51.6 Ma, respectively). Among them, the Zuowan Sb deposit is a small deposit located at about 50 km to the southeast of the Xikuangshan Sb deposit; the Laokuangshan ore block is situated to the southwest of the Daocaowan ore block in the Xikuangshan Sb deposit and has been closed (Figure 2a). Due to the lack of suitable minerals for reliable high-precision radiometric dating, it is difficult to determine the exact age of Sb mineralization in the Xikuangshan Sb deposit based on the present chronological data, but the possibility of Cenozoic Sb mineralization cannot be ruled out.

6.3. Implications for Sb Mineralization of the South China Antimony Metallogenic Belt

A potential connection between Sb mineralization and magmatism has been noted in many Sb deposits around the world [58–61]. Fu et al. [62] carried out experiments on Sb partition coefficients between magmatic fluids and silicate melts, and the results showed that Sb will only weakly partition into aqueous chloride-bearing fluid phase ($D_{Sb}^{fluid/melt}$: 0.48–0.85). It is probable that the Sb budget of large hydrothermal Sb deposits is not directly derived from magmatic fluids [62]. Additionally, stibnite samples from pure Sb and Sb-polymetallic deposits (the Banpo Sb deposit and Woxi Sb-Au-W deposit) have similar Hg isotopic compositions, suggesting a similar metal source [63]. Currently, most researchers accept a model for the genesis of Sb deposits that invokes remobilization of Sb from deep-seated Precambrian basement rocks by descending meteoric water, followed by fluid circulation and cooling into the overlying strata to form Sb orebodies [25,46,48,63–66]. Overall, for the origin of Sb(-Au-W) deposits in the South China antimony metallogenic belt, the main point of debate is whether the thermal events (heat flow) that triggered fluid migration and Sb ore deposition were caused by magmatism or tectonic movements.

The most important evidence supporting Sb mineralization triggered by magmatism is that most of the dating results for Sb(-Au-W) deposits occur in the range of ca. 160–115 Ma (Figure 9).

This is the age of the formation of high-temperature magma-related W-Sn deposits in South China during the late Mesozoic [67–69]. Previous studies have proposed that extensive intracontinental magmatism during the late Jurassic–early Cretaceous was due to the mantle upwelling that heated and remelted the lower crust [70–72]. Although late Jurassic–early Cretaceous magmatic rocks are rare in the South China antimony metallo-

genic belt (e.g., the Xiangzhong metallogenic province, Figure 1b), concealed magmas can release W-carrying fluids and contributed heat to drive the migration of deep fluids that leached Sb (with an initial δ^{123}Sb ca. −0.45‰), Au, Hg (with negative Δ^{199}Hg values), and S (with the range of δ^{34}S 6.8‰ to 10.2‰) from the Precambrian basement rock [21,22,63,73]. Locally, the ore-forming fluid ascended along deep faults and formed the mesothermal Sb mineralization at a shallow depth [28,74].

The new ages in Xikuangshan Sb deposit are temporally consistent with the younger calcite U-Pb age (ca. 60 Ma) in the Weizhai Sb deposit [10] and the apatite fission track age (ca. 61.5–27.9 Ma; apatite fission track dating was applied to the Xuefengshan Range and Yuanma Basin to constrain the Cenozoic exhumation process) [75], both of which are interpreted as uplift events in South China. The Paleogene tectonothermal event in South China may be linked to changes in the direction and speed of the subduction (ca. 60–40 Ma) of the Pacific Plate beneath the Eurasian Plate [75–77]. It is noteworthy that recent precise dating of the Indo–Asian Collision in the Tibetan Himalayan region indicates that the onset of intercontinental collision began by ca. 61 Ma [78]. At the same time, in the North Himalayan Metallogenic Belt, the Zhaxikang giant Sb-polymetallic deposit was formed (ca. 62 and 47–43 Ma) [79]. The Zhaxikang deposit is one of the representatives of regional orogenic Au-Sb deposits, and is associated with metamorphic fluid system during the syn-collision period (ca. 60–42 Ma) [79,80], and has no significant spatial relationship with pluton. Additionally, Sb mineralization of the Schlaining Sb deposit in the Eastern Alps, associated with rapid uplift during a period of Miocene (ca. 22 to 17 Ma) [65], also suggests that Sb mineralization may not be directly linked to magmatism.

In summary, we argue that the new ages (ca. 58.1, 51.9–50.4 Ma) in this study may reflect tectonothermal events during Paleogene. Fluid migration and ore deposition might be linked to high heat flow during the subduction (ca. 60–40 Ma) of the Pacific Plate beneath the Eurasian Plate and/or the Indo–Asian Collision (begun at ca. 61 Ma).

7. Conclusions

(1) The syn-stibnite calcite U-Pb age of 58.1 ± 0.9 Ma represents the timing of Sb mineralization for the calcite-stibnite veins in the Paleocene; the other three syn-stibnite calcite U-Pb ages (50.4 ± 4.4 Ma, 50.4 ± 5.0 Ma, 51.9 ± 1.6 Ma) represent the timing of Sb mineralization for the quartz-stibnite veins in the Eocene.

(2) The young in situ U-Pb ages of calcite challenge the timing of Sb mineralization in the giant Xikuangshan Sb deposit and the South China antimony metallogenic belt, which indicates the requirement for more high-precision dating studies of Sb mineralization and an emphasis on exploration of Cenozoic Sb deposits.

Supplementary Materials: The following supporting information can be downloaded at: https://www.mdpi.com/article/10.3390/min12070899/s1, Figure S1. (a) Reference materials used in the calcite in situ U-Pb dating the experiment. (b,c) Representative laser ablation craters in calcite show ideal ablation effects (under reflected light). Related to Figure 6a; Figure S2. Tera-Wasserburg concordia diagram of AHX-1d in the first U-Pb dating experiment. Related to Figures 5d and 6f; Figure S3. Tera-Wasserburg concordia diagram of PTKD-2 in the first U-Pb dating experiment. Related to Figures 5d and 6f; Figure S4. Tera-Wasserburg concordia diagram of LD-5 in the first U-Pb dating experiment. Related to Figures 5d and 6f; Figure S5. Tera-Wasserburg concordia diagram of AHX-1d in the second U-Pb dating experiment. Related to Figure 6c,d.; Figure S6. Tera-Wasserburg concordia diagram of PTKD-2 in the second U-Pb dating experiment. Related to Figure 6c,d; Figure S7. Tera-Wasserburg concordia diagram of LD-5 in the second U-Pb dating experiment. Related to Figure 6c,d.

Author Contributions: Conceptualization, J.X., X.L., J.L. and X.S.; Data curation, J.X., X.L. and X.S.; Formal analysis, J.X. and X.L.; Funding acquisition, J.X. and J.L.; Investigation, J.X., X.L., J.L. and X.S.; Methodology, J.X., X.L. and X.S.; Project administration, J.X. and J.L.; Resources, J.X. and J.L.; Software, X.L.; Supervision, J.L.; Visualization, X.L.; Writing—original draft, X.L.; Writing—review and editing, J.X., X.L., J.L., H.H., X.S., D.Z., B.L., Y.W., J.S. and X.Z. All authors have read and agreed to the published version of the manuscript.

Funding: This research is financially supported by the National Key Research and Development Plan of China (2017YFC0602402), and the National key research and development program of Hunan province (2019SK2261).

Data Availability Statement: Not applicable.

Acknowledgments: The staff of Shanxing Antimony Company and Second Team of Hunan Nonferrous Metals Geological Exploration Bureau are thanked for their help during field work.

Conflicts of Interest: The authors declare no conflict of interest.

References

1. Petty, T.R. Final List of Critical Minerals. *Fed. Regist.* **2018**, *83*, 23295–23296.
2. Jiang, S.Y.; Wen, H.J.; Xu, C.; Wang, Y.; Su, H.M.; Sun, W.D. Earth sphere cycling and enrichment mechanism of critical metals: Major scientific for future research. *Bull. Natl. Nat. Sci. Found. China* **2019**, *2*, 112–118. (In Chinese with English Abstract)
3. U.S.G.S. *Mineral Commodity Summaries 2022*; U.S. Geological Survey: Reston, VA, USA, 2022; pp. 1–202. [CrossRef]
4. Peng, J.T.; Hu, R.Z.; Lin, Y.X.; Zhao, J.H. Sm-Nd isotope dating of hydrothermal calcites from the Xikuangshan antimony deposit, Central Hunan. *Chin. Sci. Bull.* **2002**, *47*, 1134–1137. [CrossRef]
5. Peng, J.T.; Hu, R.Z.; Burnard, P.G. Samarium-neodymium isotope systematics of hydrothermal calcites from the Xikuangshan antimony deposit (Hunan, China): The potential of calcite as a geochronometer. *Chem. Geol.* **2003**, *200*, 129–136. [CrossRef]
6. Tang, Y.W.; Han, J.J.; Lan, T.G.; Gao, J.F.; Liu, L.; Xiao, C.H.; Yang, J.H. Two reliable calibration methods for accurate in situ U-Pb dating of scheelite. *J. Anal. At. Spectrom.* **2022**, *37*, 358–368. [CrossRef]
7. Peng, J.T.; Hu, R.Z.; Zhao, J.H.; Fu, Y.Z.; Lin, Y.X. Scheelite Sm-Nd dating and quartz Ar-Ar dating for Woxi Au-Sb-W deposit, western Hunan. *Chin. Sci. Bull.* **2003**, *48*, 2640–2646. [CrossRef]
8. Li, W.; Xie, G.Q.; Mao, J.W.; Wei, H.T.; Ji, Y.H.; Fu, B. Precise age constrains for the Woxi Au-Sb-W deposit, South China. *Econ. Geol.* 2022, *in press*.
9. Jin, J.F.; Tao, Y.; Lai, W.C. *Metallogenic Regularity, and Prospecting Direction of Xikuangshan-Type Sb Deposit in Central Hunan*; Sichuan Science & Technology Press: Chengdu, China, 1999. (In Chinese)
10. Luo, K.; Zhou, J.X.; Feng, Y.X.; Uysal, I.T.; Ai, N.; Zhao, J.X.; Zhang, J.W. In Situ U-Pb Dating of Calcite from the South China Antimony Metallogenic Belt. *Iscience* **2020**, *23*, 101575. [CrossRef]
11. Coogan, L.A.; Parrish, R.R.; Roberts, N.M.W. Early hydrothermal carbon uptake by the upper oceanic crust: Insight from in situ U-Pb dating. *Geology* **2016**, *44*, 147–150. [CrossRef]
12. Methner, K.; Mulch, A.; Fiebig, J.; Wacker, U.; Gerdes, A.; Graham, S.A.; Chamberlain, C.P. Rapid Middle Eocene temperature change in western North America. *Earth Planet. Sci. Lett.* **2016**, *450*, 132–139. [CrossRef]
13. Roberts, N.M.W.; Walker, R.J. U-Pb geochronology of calcite-mineralized faults: Absolute timing of rift-related fault events on the northeast Atlantic margin. *Geology* **2016**, *44*, 531–534. [CrossRef]
14. Roberts, N.M.W.; Rasbury, E.T.; Parrish, R.R.; Smith, C.J.; Horstwood, M.S.A.; Condon, D.J. A calcite reference material for LA-ICP-MS U-Pb geochronology. *Geochem. Geophys. Geosyst.* **2017**, *18*, 2807–2814. [CrossRef]
15. Goodfellow, B.W.; Viola, G.; Bingen, B.; Nuriel, P.; Kylander-Clark, A.R.C. Palaeocene faulting in SE Sweden from U-Pb dating of slickenfibre calcite. *Terra Nova* **2017**, *29*, 321–328. [CrossRef]
16. Nuriel, P.; Weinberger, R.; Kylander-Clark, A.R.C.; Hacker, B.R.; Craddock, J.P. The onset of the Dead Sea transform based on calcite age-strain analyses. *Geology* **2017**, *45*, 587–590. [CrossRef]
17. Muhammed, S.N.; Howri, M.; Kamal, K.; Axel, G.; Alain, P. U-Pb Direct Dating of Multiple Diagenetic Events in the Upper Cretaceous Carbonate Reservoir of Bekhme Formation, Kurdistan Region of Iraq, by the U-Pb Small Scale Isochron Method. In Proceedings of the GSA Annual Meeting in Seattle, Washington, DC, USA, 22–25 October 2017. [CrossRef]
18. Hagen-Peter, G.; Wang, Y.; Hints, O.; Prave, A.R.; Lepland, A. Late diagenetic evolution of Ordovician limestones in the Baltoscandian basin revealed through trace-element mapping and in situ U-Pb dating of calcite. *Chem. Geol.* **2021**, *585*, 120563. [CrossRef]
19. Xiong, S.F.; Jiang, S.Y.; Chen, Z.H.; Zhao, J.X.; Ma, Y.; Zhang, D.; Duan, Z.P.; Niu, P.P.; Xu, Y.M. A Mississippi Valley–type Zn-Pb mineralizing system in South China constrained by in situ U-Pb dating of carbonates and barite and in situ S-Sr-Pb isotopes. *GSA Bull.* **2022**. [CrossRef]
20. Kendrick, M.A.; Plümper, O.; Zhao, J.-X.; Feng, Y.; Defliese, W.F.; Müller, I.A.; Ziegler, M. Exhumation and carbonation of the Atlantis Bank core complex constrained by in situ U-Pb dating and Δ47 thermometry of calcite veins, SW Indian Ridge. *Earth Planet. Sci. Lett.* **2022**, *584*, 117474. [CrossRef]
21. Zhai, D.G.; Mathur, R.; Liu, S.A.; Liu, J.J.; Godfrey, L.; Wang, K.; Xu, J.W.; Vervoort, J. Antimony isotope fractionation in hydrothermal systems. *Geochim. Cosmochim. Acta* **2021**, *306*, 84–97. [CrossRef]
22. Fu, S.L.; Hu, R.; Batt, G.E.; Danisik, M.; Evans, N.J.; Mi, X.F. Zircon (U-Th)/He thermochronometric constraints on the mineralization of the giant Xikuangshan Sb deposit in central Hunan, South China. *Miner. Depos.* **2020**, *55*, 901–912. [CrossRef]
23. Schulz, K.J.; DeYoung, J.H., Jr.; Seal, R.R., II; Bradley, D.C. *Critical Mineral Resources of the United States—Economic and Environmental Geology and Prospects for Future Supply*; U.S. Geological Survey: Reston, VA, USA, 2017; pp. 1–797. [CrossRef]

24. Liu, H.P.; Zhang, Y.L.; Hu, W.Q. A discussion on ore genesis of the Xikuangshan Sb deposit in Hunan. *Hunan Geol.* **1985**, *1*, 28–39. (In Chinese with English Abstract)
25. Peng, J.T.; Hu, R.Z.; Deng, H.L.; Su, W.C. Strontium isotope geochemistry of the Xikuangshan antimony deposit, Central Hunan. *Geochimica* **2001**, *30*, 248–256. (In Chinese with English Abstract)
26. Fu, S.L.; Hu, R.Z.; Yin, R.S.; Yan, J.; Mi, X.F.; Song, Z.C.; Sullivan, N.A. Mercury and in situ sulfur isotopes as constraints on the metal and sulfur sources for the world's largest Sb deposit at Xikuangshan, southern China. *Miner. Depos.* **2020**, *55*, 1353–1364. [CrossRef]
27. Second Team of Hunan Nonferrous Metals Geological Exploration Bureau (STHNMGEB). *Inner Report of Deep Exploration of the Xikuangshan Sb Deposit in Huanan Province*; Second Team of Hunan Nonferrous Metals Geological Exploration Bureau: Hengyang, China, 2019. (In Chinese)
28. Hu, A.X.; Peng, J.T. Fluid inclusions and ore precipitation mechanism in the giant Xikuangshan mesothermal antimony deposit, South China: Conventional and infrared microthermometric constraints. *Ore Geol. Rev.* **2018**, *95*, 49–64. [CrossRef]
29. Wu, L.S.; Hu, X.W. Xikuangshan mica-plagioclase lamprophyre and its granite inclusions, Hunan Province. *Geol. Geochem.* **2000**, *28*, 51–55. (In Chinese with English Abstract)
30. Hu, A.X.; Peng, J.T. Mesozoic lamprophyre and its origin in the Xikuangshan mining district, central Hunan. *Acta Petrol. Sin.* **2016**, *32*, 2041–2056. (In Chinese with English abstract)
31. Liu, G.M.; Jian, H.M. Geological characteristics of the Xikuangshan antimony ore field. *Miner. Depos.* **1983**, *2*, 43–49. (In Chinese with English Abstract)
32. Second Team of Hunan Nonferrous Metals Geological Exploration Bureau (STHNMGEB). *Report of Mineral Prospecting of the Daocaowan Sb Ore Block in Huanan Province*; Second Team of Hunan Nonferrous Metals Geological Exploration Bureau: Hengyang, China, 2015. (In Chinese)
33. Xikuangshan Mine. *Chorography of Xikuangshan Mine*; Xikuangshan Mining Administration: Lengshuijiang, China, 1983. (In Chinese)
34. Wen, G.Z.; Wu, Q.; Liu, H.Y.; Xie, G.Z.; Lei, X.L. Preliminary study on ore controlling regularities and metallogenic mechanism of super large-sized Sb-deposits in Xikuangshan. *Geol. Prospect.* **1993**, *29*, 20–27. (In Chinese with English Abstract)
35. Hu, X.W. The Geological Setting and Genesis of Xikuangshan Super-Giant Antimony Deposits, Hunan Province, China. Ph.D. Thesis, Chinese Academy of Geological Sciences, Beijing, China, 1995. (In Chinese)
36. Woodhead, J.D.; Hergt, J.M. Strontium, neodymium and lead isotope analyses of NIST glass certified reference materials: SRM 610, 612, 614. *Geostand. Newsl. -J. Geostand. Geoanal.* **2001**, *25*, 261–266. [CrossRef]
37. Kylander-Clark, A.R.C. Expanding limits of laser-ablation U-Pb calcite geochronology. *Geochronology* **2020**, *2*, 343–354. [CrossRef]
38. Liu, E.T.; Zhao, J.X.; Pan, S.Q.; Yan, D.T.; Lu, J.; Hao, S.B.; Gong, Y.; Zou, K. A new technology of basin fluid geochronology: In-situ U-Pb dating of calcite. *Earth Sci.* **2019**, *44*, 698–712. (In Chinese with English Abstract) [CrossRef]
39. Shen, A.J.; Hu, A.P.; Cheng, T.; Liang, F.; Pan, W.Q.; Feng, Y.X.; Zhao, J.X. Laser ablation in situ U-Pb dating and its application to diagenesis-porosity evolution of carbonate reservoirs. *Pet. Explor. Dev.* **2019**, *46*, 1127–1140. [CrossRef]
40. Cheng, T.; Zhao, J.X.; Feng, Y.X.; Pan, W.Q.; Liu, D.Y. In-situ LA-MC-ICPMS U-Pb dating method for low-uranium carbonate minerals. *Chin. Sci. Bull.* **2020**, *65*, 150–154. [CrossRef]
41. Hu, X.W.; Pei, R.F.; Su, Z. Sm-Nd dating for antimony mineralization in the Xikuangshan deposit, Hunan, China. *Resour. Geol.* **1996**, *46*, 227–231.
42. Xiao, X.G. Geochronlogy, Ore Geochemistry, and Genesis of the Banpo Antimony Deposit, Guizhou Province, China. Ph.D. Thesis, Kunming University of Science and Technology, Kunming, China, 2014. (In Chinese)
43. Zhu, L.M. Elemental Association and Fractionation Mechanisms of Low Temperature Metallogenic Domain on the Southwest Margin of the Yangtze Block (Guizhou Province). Ph.D. Thesis, Institution of Chinese Academy of Sciences, Beijing, China, 1998. (In Chinese)
44. Wang, Z.P. Genesis and Dynamic Mechanism of the Epithermal Ore Deposits, SW Guizhou, China—A Case Study of Gold and Antimony Deposits. Unpublished Ph.D. Thesis, Institute of Geochemistry, Chinese Academy of Sciences, Guiyang, China, 2013. (In Chinese)
45. Wang, J.S. Mineralization, Chronology and Dynamic Research of Low Temperature Metallogenic Domain, Southwest China. Ph.D. Thesis, Institute of Geochemistry, Chinese Academy of Science, Beijing, China, 2012. (In Chinese)
46. Li, H.; Danisik, M.; Zhou, Z.K.; Jiang, W.C.; Wu, J.H. Integrated U-Pb, Lu-Hf and (U-Th)/He analysis of zircon from the Banxi Sb deposit and its implications for the low-temperature mineralization in South China. *Geosci. Front.* **2020**, *11*, 1323–1335. [CrossRef]
47. Fu, S.L.; Hu, R.Z.; Yan, J.; Lan, Q.; Gao, W. The mineralization age of the Banxi Sb deposit in Xiangzhong metallogenic province in southern China. *Ore Geol. Rev.* **2019**, *112*, 103033. [CrossRef]
48. Li, H.; Wu, Q.H.; Evans, N.J.; Zhou, Z.K.; Kong, H.; Xi, X.S.; Lin, Z.W. Geochemistry and geochronology of the Banxi Sb deposit: Implications for fluid origin and the evolution of Sb mineralization in central-western Hunan, South China. *Gondwana Res.* **2018**, *55*, 112–134. [CrossRef]
49. Wang, X.K. *Guizhou Dushan Antimony Deposit Geology*; Yunnan Science and Technology Press: Kunming, China, 1994. (In Chinese)
50. Wei, W.Z. Geological characteristics of the Maxiong antimony deposit. *Southwest China Ore Depos. Geol.* **1993**, *7*, 8–16. (In Chinese with English Abstract)

51. Shi, M.K.; Fu, B.Q.; Jin, X.X.; Zhou, X.C. *Antimony Metallogeny in the Central Part of Hunan Province*; Hunan Science & Technology Press: Changsha, China, 1993. (In Chinese)
52. Hu, R.Z.; Peng, J.T.; Ma, D.S.; Su, W.C.; Shi, C.H.; Bi, X.W.; Tu, G.C. Epoch of large-scale low-temperature mineralizations in southwestern Yangtze massif. *Mineral. Depos.* **2007**, *26*, 583–596. (In Chinese with English Abstract)
53. Wang, Y.L.; Chen, Y.C.; Wang, D.H.; Xu, Y.; Chen, Z.H. Scheelite Sm-Nd dating of the Zhazixi W-Sb deposit in Hunan and its geological significance. *Geol. China* **2012**, *39*, 1339–1344. (In Chinese with English Abstract)
54. Shen, N.P. Geochemistry and Metallogenic Mechanism of the Xujiashan Antimony Deposit in Hubei Province, China. Ph.D. Thesis, Institution of Geochemistry, Chinese Academy of Sciences, Beijing, China, 2008. (In Chinese)
55. Peng, J.T.; Dai, T.G. On the mineralization epoch of the Xuefeng gold metallogenic province. *Geol. Prospect.* **1998**, *34*, 37–41. (In Chinese with English Abstract)
56. Dickin, A.P. *Radiogenic Isotope Geology*, 2nd ed.; Cambridge University Press: Cambridge, UK, 2005; pp. 1–509.
57. Li, W.; Xie, G.Q.; Cook, N.J.; Mao, J.W.; Li, C.; Ciobanu, C.L.; Zhang, Z.Y. Tracking dynamic hydrothermal processes: Textures, in-situ Sr-Nd isotopes, and trace-element analysis of scheelite from the Yangjiashan vein-type W deposit, South China. *Am. Mineral.* **2021**, *106*, 1987–2002. [CrossRef]
58. Dill, H.G.; Melcher, F.; Botz, R. Meso- to epithermal W-bearing Sb vein-type deposits in calcareous rocks in western Thailand; with special reference to their metallogenetic position in SE Asia. *Ore Geol. Rev.* **2008**, *34*, 242–262. [CrossRef]
59. Pavlova, G.G.; Borisenko, A.S.; Goverdovskii, V.A.; Travin, A.V.; Zhukova, I.A.; Tret'yakova, I.G. Permian-Triassic magmatism and Ag-Sb mineralization in southeastern Altai and northwestern Mongolia. *Russ. Geol. Geophys.* **2008**, *49*, 545–555. [CrossRef]
60. Pavlova, G.G.; Borisenko, A.S. The age of Ag-Sb deposits of Central Asia and their correlation with other types of ore systems and magmatism. *Ore Geol. Rev.* **2009**, *35*, 164–185. [CrossRef]
61. Němec, M.; Zachariáš, J. The Krásná Hora, Milešov, and Příčovy Sb-Au ore deposits, Bohemian Massif: Mineralogy, fluid inclusions, and stable isotope constraints on the deposit formation. *Miner. Depos.* **2018**, *53*, 225–244. [CrossRef]
62. Fu, S.; Zajacz, Z.; Tsay, A.; Hu, R. Can magma degassing at depth donate the metal budget of large hydrothermal Sb deposits? *Geochim. Cosmochim. Acta* **2020**, *290*, 1–15. [CrossRef]
63. Deng, C.Z.; Zhang, J.W.; Hu, R.Z.; Luo, K.; Zhu, Y.N.; Yin, R.S. Mercury isotope constraints on the genesis of late Mesozoic Sb deposits in South China. *Sci. China-Earth Sci.* **2022**, *65*, 269–281. [CrossRef]
64. Peng, B.; Frei, R. Nd-Sr-Pb isotopic constraints on metal and fluid sources in W-Sb-Au mineralization at Woxi and Liaojiaping (Western Hunan, China). *Miner. Depos.* **2004**, *39*, 313–327. [CrossRef]
65. Sosnicka, M.; de Graaf, S.; Morteani, G.; Banks, D.A.; Niedermann, S.; Stoltnow, M.; Lueders, V. The Schlaining quartz-stibnite deposit, Eastern Alps, Austria: Constraints from conventional and infrared microthermometry and isotope and crush-leach analyses of fluid inclusions. *Miner. Depos.* **2022**, *57*, 725–741. [CrossRef]
66. Ding, J.H.; Zhang, Y.; Ma, Y.B.; Wang, Y.; Zhang, J.B.; Zhang, T.T. Metallogenic characteristics and resource potential of antimony in China. *J. Geochem. Explor.* **2021**, *230*, 106834. [CrossRef]
67. Hu, R.Z.; Fu, S.L.; Huang, Y.; Zhou, M.F.; Fu, S.H.; Zhao, C.H.; Wang, Y.J.; Bi, X.W.; Xiao, J.F. The giant South China Mesozoic low-temperature metallogenic domain: Reviews and a new geodynamic model. *J. Asian Earth Sci.* **2017**, *137*, 9–34. [CrossRef]
68. Mao, J.W.; Ouyang, H.G.; Song, S.W.; Santosh, M.; Yuan, S.D.; Zhou, Z.H.; Zheng, W.; Liu, H.; Liu, P.; Cheng, Y.B.; et al. Geology and metallogeny of tungsten and tin deposits in China. *Soc. Econ. Geol. Spec. Publ.* **2019**, *22*, 411–482.
69. Xu, J.W.; Lai, J.Q.; Li, B.; Lu, A.H.; Rocholl, A.; Dick, J.M.; Peng, J.T.; Wang, K.L. Tungsten mineralization during slab subduction: A case study from the Huxingshan deposit in northeastern Hunan Province, South China. *Ore Geol. Rev.* **2020**, *124*, 103657. [CrossRef]
70. Li, Z.X.; Li, X.H. Formation of the 1300-km-wide intracontinental orogen and postorogenic magmatic province in Mesozoic South China: A flat-slab subduction model. *Geology* **2007**, *35*, 179–182. [CrossRef]
71. Huang, H.Q.; Li, X.H.; Li, W.X.; Li, Z.X. Formation of high delta O-18 fayalite-bearing A-type granite by high-temperature melting of granulitic metasedimentary rocks, southern China. *Geology* **2011**, *39*, 903–906. [CrossRef]
72. Mao, J.W.; Zheng, W.; Xie, G.Q.; Lehmann, B.; Goldfarb, R. Recognition of a Middle-Late Jurassic arc-related porphyry copper belt along the southeast China coast: Geological characteristics and metallogenic implications. *Geology* **2021**, *49*, 592–596. [CrossRef]
73. Yang, R.Y.; Ma, D.S.; Pan, J.Y. Research on thermal field of ore-forming fluid of Xikuangshan Sn deposit in Central Hunan. *Geochimica* **2003**, *6*, 509–519. (In Chinese with English Abstract) [CrossRef]
74. Zhang, L.; Yang, L.Q.; Groves, D.I.; Sun, S.C.; Liu, Y.; Wang, J.Y.; Li, R.H.; Wu, S.G.; Gao, L.; Guo, J.L.; et al. An overview of timing and structural geometry of gold, gold-antimony and antimony mineralization in the Jiangnan Orogen, southern China. *Ore Geol. Rev.* **2019**, *115*, 103173. [CrossRef]
75. Wang, Y.M.; Zhang, J.; Zhang, B.H.; Zhao, H. Cenozoic exhumation history of South China: A case study from the Xuefeng Mt. Range. *J. Asian Earth Sci.* **2018**, *151*, 173–189. [CrossRef]
76. Li, X.M.; Wang, Y.J.; Tan, K.X.; Peng, T.P. Meso-Cenozoic uplifting and exhumation on Yunkaidashan: Evidence from fission track thermochronology. *Chin. Sci. Bull.* **2005**, *9*, 903–909. [CrossRef]
77. Tang, S.L.; Yan, D.P.; Qiu, L.; Gao, J.F.; Wang, C.L. Partitioning of the Cretaceous Pan-Yangtze Basin in the central South China Block by exhumation of the Xuefeng Mountains during a transition from extensional to compressional tectonics? *Gondwana Res.* **2014**, *25*, 1644–1659. [CrossRef]

78. An, W.; Hu, X.M.; Garzanti, E.; Wang, J.G.; Liu, Q. New Precise Dating of the India-Asia Collision in the Tibetan Himalaya at 61 Ma. *Geophys. Res. Lett.* **2021**, *48*, e2020GL090641. [CrossRef]
79. Wang, D.; Zheng, Y.Y.; Mathur, R.; Jiang, J.S.; Zhang, S.K.; Zhang, J.F.; Yu, M. Multiple mineralization events in the Zhaxikang Sb-Pb-Zn-Ag deposit and their relationship with the geodynamic evolution in the North Himalayan Metallogenic Belt, South Tibet. *Ore Geol. Rev.* **2019**, *105*, 201–215. [CrossRef]
80. Wang, D.; Mathur, R.; Zheng, Y.Y.; Qiu, K.F.; Wu, H.J. Redox-controlled antimony isotope fractionation in the epithermal system: New insights from a multiple metal stable isotopic combination study of the Zhaxikang Sb-Pb-Zn-Ag deposit in Southern Tibet. *Chem. Geol.* **2021**, *584*, 120541. [CrossRef]